CrossMark

TECHNICAL ARTICLE

Crystal structures of tricalcium citrates

James A. Kaduk[1,2,a)]
[1]*Illinois Institute of Technology, 3101 S. Dearborn St., Chicago, Illinois 60616*
[2]*North Central College, 131 S. Loomis St., Naperville, Illinois 60540*

(Received 20 November 2017; accepted 11 February 2018)

The crystal structures of calcium citrate hexahydrate, calcium citrate tetrahydrate, and anhydrous calcium citrate have been solved using laboratory and synchrotron X-ray powder diffraction data, and optimized using density functional techniques. Both the hexahydrate and tetrahydrate structures are characterized by layers of edge-sharing Ca coordination polyhedra, including triply chelated Ca. An additional isolated Ca is coordinated by water molecules, and two uncoordinated water molecules occur in the hexahydrate structure. The previously reported polymorph of the tetrahydrate contains the same layers, but only two H_2O coordinated to the isolated Ca and two uncoordinated water molecules. Anhydrous calcium citrate has a three-dimensional network structure of Ca coordination polyhedra. The new polymorph of calcium citrate tetrahydrate is the major crystalline phase in several commercial calcium supplements. © *2018 International Centre for Diffraction Data.*
[doi:10.1017/S0885715618000283]

Key words: calcium citrate, powder diffraction, Rietveld refinement, density functional theory

I. INTRODUCTION

Calcium citrate (as the tetrahydrate) is a common dietary calcium supplement, as well as a food additive. It is supposed to be more bioavailable than calcium carbonate when used as a calcium supplement (Tondapu *et al.*, 2009). Calcium citrate is an intermediate in the isolation of citric acid from the fermentation process by which citric acid is produced industrially. The citric acid in the broth is neutralized by the addition of calcium hydroxide, precipitating calcium citrate.

Calcium citrate tetrahydrate has been observed as the mineral earlandite in an unconsolidated ocean floor sediment from the Weddell Sea near Antarctica (Bannister, 1936). A powder pattern of earlandite is included in the Powder Diffraction File (Fawcett *et al.*, 2017) as entry 00-028-2003; the source is a private communication from Monsanto. A monoclinic unit cell was reported by Poganis and Shaw (1957). A triclinic crystal structure of calcium citrate tetrahydrate has been reported only recently (Herdtweck *et al.*, 2011), from a hydrothermally synthesized pseudomerohedrally-twinned crystal at 123 K. The structure is included in the Cambridge Structural Database (Groom *et al.*, 2016) as Refcode ISEQIH. A powder pattern calculated from this crystal structure is included in the Powder Diffraction File as entry 01-084-5956. The Herdtweck paper also reports a Rietveld refinement using room-temperature powder data.

Although a search of the powder patterns of three commercial calcium supplements against the PDF (subject to the filter C, H, O, and Ca only) yields the entry 00-028-2003 as a hit, the similarity of the patterns to the database entry is not particularly good (Figure 1). The major phase in the supplements does *not* match the pattern calculated from the ISEQIH structure, even though it appears to be present in two of the supplements as a minor phase. To carry out quantitative phase analyses of these tablets, the crystal structure of the major form of calcium citrate tetrahydrate had to be determined.

II. EXPERIMENTAL

Supplements

Citracal + D_3, Walgreen's calcium citrate, and Century calcium citrate were purchased from local pharmacies. The tablets were ground in a mortar and pestle, sieved to <325 mesh, and packed into 0.7 mm glass capillaries, which were sealed with petroleum jelly. The powder patterns were measured on a PANalytical Empyrean diffractometer equipped with an incident-beam focusing mirror and an X'Celerator detector. The patterns (1°–50° 2θ, 0.0167113° steps, 4 s step^{-1}, 1/4° divergence slit, 0.02 rad Soller slits) were measured from rotated capillaries using Mo$K\alpha$ radiation.

$Ca_3(C_6H_5O_7)_2(H_2O)_6$

Calcium carbonate (1.5028 g, 15.0 mmoles) was added to a solution of 2.0759 g citric acid monohydrate (10.0 mmoles) in 8 mL distilled water. After the fizzing of the reaction, the clear colorless solution was evaporated at ambient conditions. The yield of white solid was 2.4890 g, which corresponded to the hexahydrate. The thermogravimetric analysis also confirmed the compound as the hexahydrate; the water loss occurred in two steps, at approximately 80 and 140 °C. A powder pattern was measured on a Bruker D2 Phaser diffractometer equipped with a LynxEye position-sensitive detector (5°–70° 2θ, 0.0202144° steps, 0.5 s step^{-1}, 0.6° divergence slit, 2.5° Soller slits, 3 mm scatter screen height) using Cu$K\alpha$ radiation. This pattern could be indexed on a *C*-centered monoclinic unit cell having $a = 21.424$, $b = 6.344$, $c = 17.316$ Å, $\beta = 109.30°$,

a)Author to whom correspondence should be addressed. Electronic mail: kaduk@polycrystallography.com

https://doi.org/10.1017/S0885715618000283 Published online by Cambridge University Press

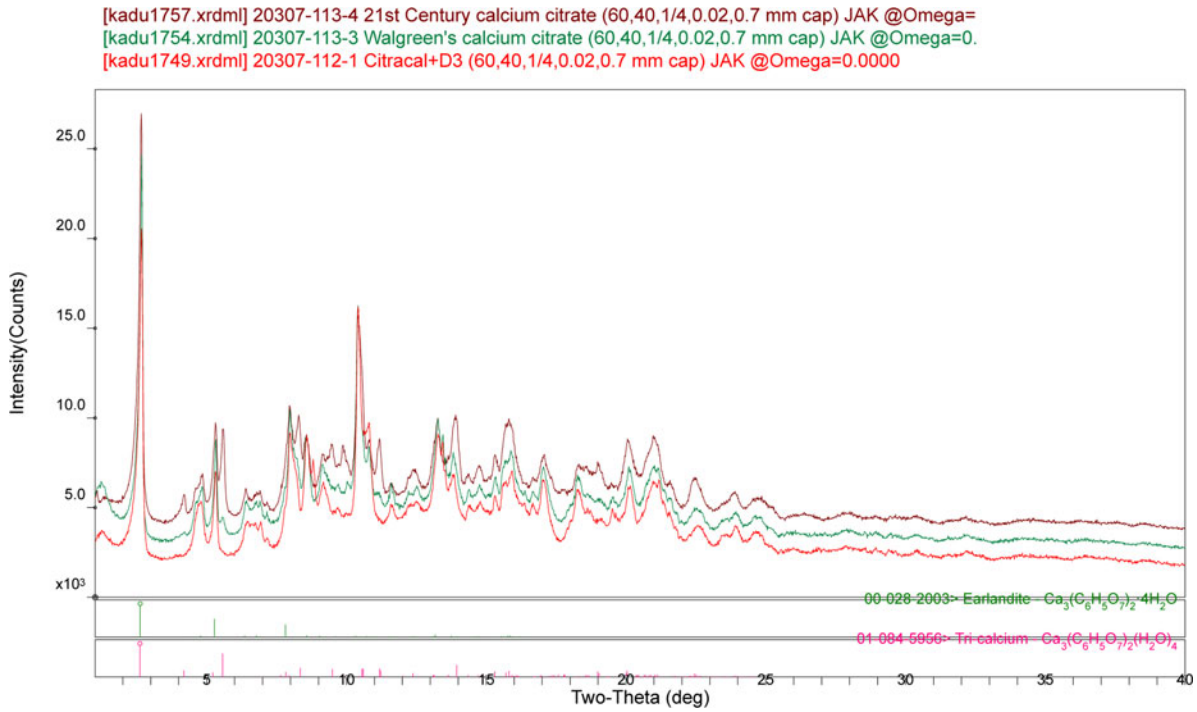


Figure 1. (Colour online) Comparison of the powder patterns of three commercial calcium citrate supplements and the PDF entries for calcium citrate tetrahydrate.

and $V = 2234.37$ Å^3, but structure solution was unsuccessful (because this was the wrong unit cell).

The white powder was packed into a 1.5 mm diameter Kapton capillary and rotated during the measurement at ~50 cycles s^{-1}. The powder pattern was also measured at 295 K at beam line 11-BM (Lee *et al.*, 2008; Wang *et al.*, 2008) of the Advanced Photon Source at Argonne National Laboratory using a wavelength of 0.413357 Å from 0.5° to 50° 2θ with a step size of 0.001° and a counting time of 0.1 s step^{-1}. The pattern was indexed on a *C*-centered monoclinic unit cell having $a = 33.015$, $b = 10.777$, $c = 5.957$ Å, $\beta = 91.71$°, $V = 2118.4$ Å^3, and $Z = 4$ using Jade (MDI, 2016). Analysis of the systematic absences using EXPO2014 (Altomare *et al.*, 2013) suggested the space groups *Cc* and *C*2/*c*. *C*2/*c* was assumed, and was confirmed by successful solution and refinement of the structure. A reduced cell search in the Cambridge Structural Database (Groom *et al.*, 2016) combined with the chemistry "C H O Ca only" yielded only poly[μ_3-succinatocalcium(II)], $[Ca(C_4H_5O_4)]_n$ (Mazaj *et al.*, 2012; Refcode XAQJIK). The structure was solved by direct methods using EXPO2014.

Rietveld refinement was carried out using GSAS (Toby, 2001; Larson and Von Dreele, 2004). Only the 2.0°–35.0° portion of the pattern was included in the refinement ($d_{min} = 0.687$ Å). All non-H bond distances and angles were subjected to restraints. The C–C bonds between the terminal carboxyl carbon atoms and the adjacent carbon atoms were restrained at 1.51(1) Å, the C–C bonds between the central carbon atom and the adjacent carbon atoms at 1.54(1) Å, the C–C bond between the central carbon atom and the central carboxyl carbon at 1.55(1) Å, the C–O bond to the hydroxy group at 1.42(2) Å, and the C–O bonds in the carboxylate groups at 1.27(2) Å. The tetrahedral carbon bond angles were restrained at 109(3)°, and the angles in the planar carboxyl groups at 120(3)°. The hydrogen atoms were included at fixed positions, which were recalculated during the course of the refinement using Materials Studio (Dassault, 2014). The Ca–O distances were not restrained. The restraints contributed 1.1% to the final χ^2. The U_{iso} of the non-H atoms were grouped by chemical similarity. The U_{iso} of each citrate hydrogen atom was fixed at 1.3× that of the heavy atom to which it was attached. The peak profiles were described using profile function #4 (Thompson *et al.*, 1987; Finger *et al.*, 1994), which includes the Stephens (1999) anisotropic strain broadening model. The background was modeled using a three-term shifted Chebyshev polynomial, with a four-term diffuse scattering function to model the Kapton capillary and any amorphous component. A sixth-order spherical harmonic model was included; the refined texture index was only 1.004, so preferred orientation was not significant. A few weak peaks were not accounted for by the major phase. They corresponded to calcite, which was included in the refinement and its concentration refined to 0.9 wt%. The final refinement of 94 variables using 33 032 observations (33 003 data points and 29 restraints) yielded the residuals $R_{wp} = 0.0774$, $R_p = 0.0618$, and $\chi^2 = 3.188$. The largest peak (0.06 Å from Ca19) and hole (1.64 Å from O21) in the difference Fourier map were 0.35 and −0.20 eÅ^{-3}, respectively. The Rietveld plot is included as Figure 2(a). The largest errors in the fit are in the shapes of some of the low-angle peaks.

$Ca_3(C_6H_5O_7)_2(H_2O)_4$

Reagent calcium citrate tetrahydrate was purchased from Avocado Research Chemicals Ltd. (lot #C8307A) and Aldrich Chemical Co. (lot # 15421BO). The peaks from the Avocado sample were narrower, so that pattern was used for structure solution and refinement. The powder was ground

https://doi.org/10.1017/S0885715618000283 Published online by Cambridge University Press

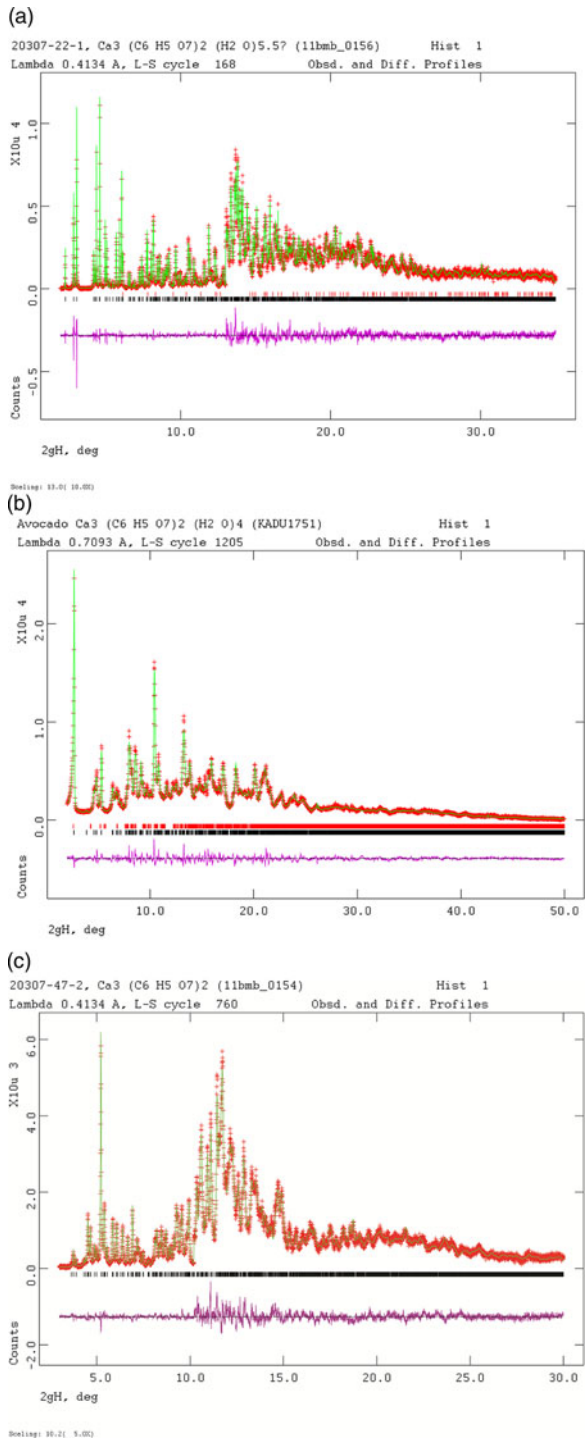


Figure 2. (Colour online) (a) The Rietveld plot for the refinement of calcium citrate hexahydrate. The red crosses represent the observed data points, and the green line is the calculated pattern. The magenta curve is the difference pattern, plotted at the same vertical scale as the other patterns. The vertical scale has been multiplied by a factor of 10 for 2θ >13.0°. (b) The Rietveld plot for the refinement of the new form of calcium citrate tetrahydrate. The red crosses represent the observed data points, and the green line is the calculated pattern. The magenta curve is the difference pattern, plotted at the same vertical scale as the other patterns. The row of black tick marks indicates the calculated reflection positions for the new form, and the red tick marks indicate peaks from the 1% ISEQIH impurity. (c) The Rietveld plot for the refinement of anhydrous calcium citrate. The red crosses represent the observed data points, and the green line is the calculated pattern. The magenta curve is the difference pattern, plotted at the same vertical scale as the other patterns. The vertical scale has been multiplied by a factor of 5 for 2θ >10.2°.

in a mortar and pestle, sieved to <325 mesh, packed into a 0.7 mm glass capillary, and sealed with petroleum jelly. The powder pattern was measured on a PANalytical Empyrean diffractometer equipped with an incident-beam focusing mirror and an X'Celerator detector. The pattern (1–50° 2θ, 0.0167113° steps, 4 s step^{-1}, 1/4° divergence slit, 0.02 radian Soller slits) was measured from a rotated capillary using Mo$K\alpha$ radiation.

The relatively broad peaks [FWHM (full-width at half-maximum) ~0.10°–0.15°] and extensive peak overlap made this a difficult pattern to index. After many trials, several algorithms settled on the same triclinic cell, with $a = 5.905$, $b = 10.463$, $c = 15.416$ Å, $\alpha = 93.496$, $\beta = 95.736$, $\gamma = 90.602°$, $V = 954.8$ Å^3, and $Z = 2$. The space group was assumed to be P-1, which was confirmed by successful solution and refinement of the structure. A reduced cell search (2% tolerance) in the Cambridge Structural Database (Groom *et al.*, 2016) combined with the chemistry "C H O Ca only" yielded no hits.

Many attempts to solve the structure by direct methods, charge flipping, and Monte Carlo simulated annealing using independent Ca and citrate fragments were unsuccessful. Eventually, it was realized that the unit cell was similar to (and smaller than) the reduced cell of the C-centered monoclinic cell of the hexahydrate: $a = 5.9570$, $b = 10.7728$, $c = 17.3590$ Å, $\alpha = 108.07$, $\beta = 91.62$, and $\gamma = 90.00°$. The transformation matrix is [0 0 1/0–1 0/½ ½ 0]. Using Materials Studio, the hexahydrate structure was transformed to the reduced cell. The two non-coordinated water molecules were removed, and the lattice parameters were changed to the observed values for the tetrahydrate. The structure was optimized using Forcite (fixed cell), and the Rietveld refinement was begun from this model.

Rietveld refinement was carried out using GSAS (Toby, 2001; Larson and Von Dreele, 2004). Only the 2.0–50.0° portion of the pattern was included in the refinement (d_{min} = 0.839 Å). All non-H bond distances and angles were subjected to restraints. The C–C bonds between the terminal carboxyl carbon atoms and the adjacent carbon atoms were restrained at 1.51(2) Å, the C–C bonds between the central carbon atom and the adjacent carbon atoms at 1.54(1) Å, the C–C bond between the central carbon atom and the central carboxyl carbon at 1.55(1) Å, the C–O bond to the hydroxyl group at 1.43(3) Å, and the C–O bonds in the carboxylate groups at 1.25(2) Å. The tetrahedral carbon bond angles were restrained at 109(3)°, and the angles in the planar carboxyl groups at 120 (3)°. The hydrogen atoms were included at fixed positions, which were recalculated during the course of the refinement using Materials Studio (Dassault, 2014). The Ca–O distances were restrained to 2.43(10) Å, and non-bonded O···O distance restraints were applied to the water molecules in the Ca39 coordination sphere. The restraints contributed 22.7% to the final χ^2. The main deviations from the restrained values are in the Ca–O distances and the O–C–O carboxylate angles, which we expect to be more variable. A common U_{iso} was refined for the Ca atoms, but the U_{iso} of the other non-H atoms were fixed at reasonable values. The U_{iso} of each hydrogen atom was fixed at 1.3× that of the heavy atom to which it was attached. The peak profiles were described using profile function #4 (Thompson *et al.*, 1987; Finger *et al.*, 1994), which includes the Stephens (1999) anisotropic strain

https://doi.org/10.1017/S0885715618000283 Published online by Cambridge University Press

broadening model. The background was modeled using a one-term shifted Chebyshev polynomial, with a seven-term diffuse scattering function to model the glass capillary and any amorphous component. An eighth-order spherical harmonic model was included; the refined texture index was 1.824, so preferred orientation was significant. ISEQIH was included as a second phase, and its concentration refined to 1.2 wt%. The final refinement of 155 variables using 2959 observations (2871 data points and 88 restraints) yielded the residuals R_{wp} = 0.0543, R_p = 0.0423, and χ^2 = 10.37. The largest peak (1.79 Å from O15) and hole (at Ca19 and Ca20) in the difference Fourier map were 3.71 and −6.40 eÅ^{-3}, respectively. The Rietveld plot is included as Figure 2(b). The overall fit is excellent; the good signal/noise and the restraints result in a relatively high reduced χ^2 to accompany the low R_{wp}. The largest errors in the fit are in the shapes of some of the peaks.

$Ca_3(C_6H_5O_7)_2$

An aliquot of Sigma-Aldrich calcium citrate tetrahydrate was heated in air from 20 to 260 °C at 8.5 °C min^{-1}, and held at 260° for 33 min. The resulting white powder was transferred to a sealed glass jar to cool. A powder pattern was measured on a Bruker D2 Phaser diffractometer equipped with a LynxEye position-sensitive detector (5–70° 2θ, 0.0202144° steps, 0.5 s step^{-1}, 0.6° divergence slit, 2.5° Soller slits, 3 mm scatter screen height) using Cu$K\alpha$ radiation. This pattern could be indexed on a primitive monoclinic unit cell having a = 12.161, b = 10.251, c = 14.034 Å, β = 95.62°, and V = 1741.33 Å^3.

The white powder was packed into a 1.5 mm diameter Kapton capillary and rotated during the measurement at ~50 cycles s^{-1}. The powder pattern was also measured at 295 K at beam line 11-BM (Lee *et al.*, 2008; Wang *et al.*, 2008) of the Advanced Photon Source at Argonne National Laboratory using a wavelength of 0.413357 Å from 0.5° to 50° 2θ with a step size of 0.001° and a counting time of 0.1 s step^{-1}. Both N-TREOR incorporated into EXPO2014 (Altomare *et al.*, 2013) and Jade (MDI, 2016) yielded the same triclinic unit cell having a = 6.103, b = 10.483, c = 13.131 Å, α = 111.75, β = 90.36, γ = 92.00°, V = 779.64 Å^3, and Z = 2. The space group was assumed to be P-1, which was confirmed by successful solution and refinement. A reduced cell search (2% tolerance) in the Cambridge Structural Database (Groom *et al.*, 2016) combined with the chemistry "C H O Ca only" yielded the structures of calcium formate, but no other hits.

Many attempts to solve the structure by direct methods, charge flipping, and Monte Carlo simulated annealing using independent Ca and citrate fragments were unsuccessful. The successful strategy was to extract a $Ca_3(C_6H_5O_7)_2$ fragment from the structure of $Ca_3(C_6H_5O_7)_2(H_2O)_6$, and remove the Ca–O chelation bonds, leaving each Ca bonded to only one O. This complex fragment was used to solve the structure with FOX (Favre-Nicolin & Černý, 2002). The structure was optimized using the (force field) Forcite module of Materials Studio (Dassault, 2014) to begin the Rietveld refinement. The final refinement was started from the result of the density functional theory (DFT) calculation.

Rietveld refinement was carried out using GSAS (Toby, 2001; Larson and Von Dreele, 2004). Only the 3.0°–30.0° portion of the pattern was included in the refinement (d_{min} = 0.798 Å). The lowest-angle portion of the pattern was shadowed by the beam stop, and the asymmetry of the lowest-angle peak was difficult to model. To avoid bias from an incorrect intensity, this peak was excluded. All non-H bond distances and angles were subjected to restraints. The C–C bonds between the terminal carboxyl carbon atoms and the adjacent

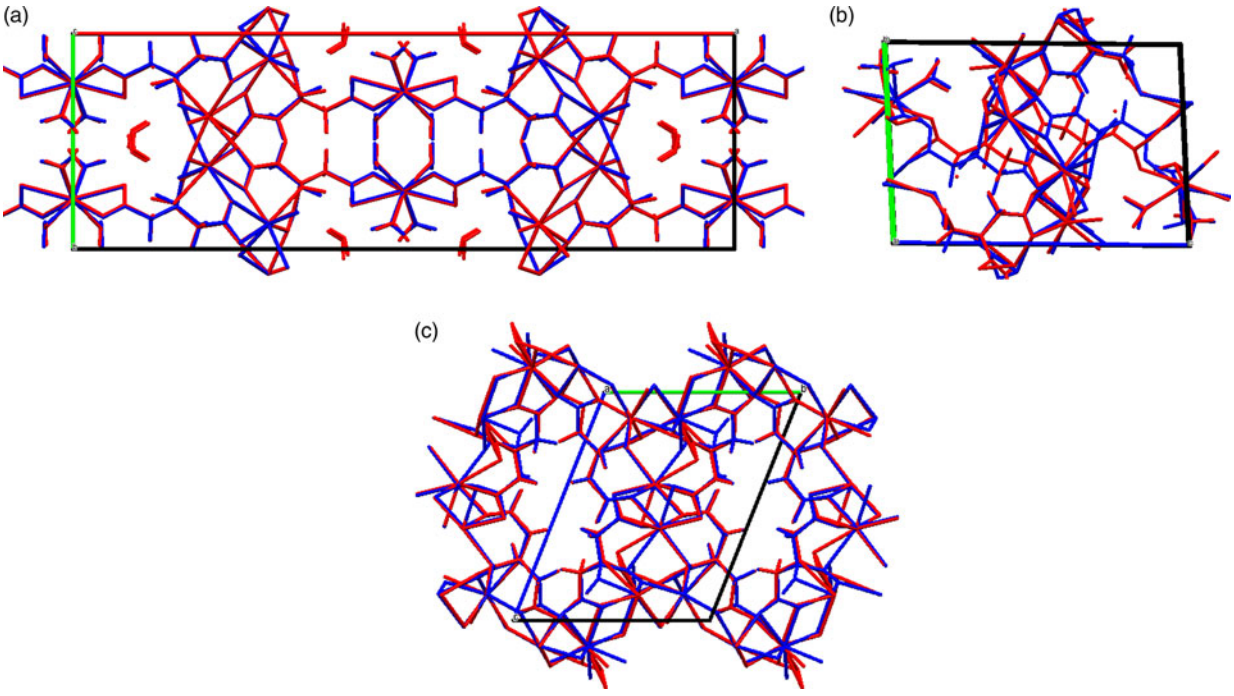


Figure 3. (Colour online) (a) Comparison of the refined and optimized structures of calcium citrate hexahydrate. The Rietveld refined structure is in red, and the DFT-optimized structure is in blue. (b) Comparison of the refined and optimized structures of the new form of calcium citrate tetrahydrate. The Rietveld refined structure is in red, and the DFT-optimized structure is in blue. (c) Comparison of the refined and optimized structures of anhydrous calcium citrate. The Rietveld refined structure is in red, and the DFT-optimized structure is in blue.

https://doi.org/10.1017/S0885715618000283 Published online by Cambridge University Press

TABLE I. Triclinic (P-1) lattice parameters of $Ca_3(C_6H_5O_7)_2(H_2O)_4$.

Polymorph Temperature (K)	ISEQIH 123	ISEQIH Ambient	This work 300
a, (Å)	5.9466(4)	5.985	5.9206(14)
b (Å)	10.2247(8)	10.257	10.5133(23)
c (Å)	16.6496(13)	16.668	15.4730(22)
α (°)	72.213(7)	72.380	93.200(21)
β (°)	79.718(7)	80.085	95.503(18)
γ (°)	89.791(6)	89.869	89.647(20)
V (Å^3)	947.06(13)	959.3	957.18(33)
ΔV (%)	−1.3	0	−0.2

carbon atoms were restrained at 1.51(1) Å, the C–C bonds between the central carbon atom and the adjacent carbon atoms at 1.54(1) Å, the C–C bond between the central carbon atom and the central carboxyl carbon at 1.55(1) Å, the C–O bond to the hydroxy group at 1.42(2) Å, and the C–O bonds in the carboxylate groups at 1.27(2) Å. The tetrahedral carbon bond angles were restrained at 109(3)°, and the angles in the planar carboxyl groups at 120(3)°. The hydrogen atoms were included at fixed positions, which were recalculated during the course of the refinement using Materials Studio (Dassault, 2014). The Ca–O distances were not restrained. The restraints contributed 12.4% to the final χ^2; the deviations from the restrained values were widely distributed among the geometrical parameters. The U_{iso} of the non-H atoms were grouped by chemical similarity. The U_{iso} of the hydrogen atoms were fixed at a reasonable value. The peak profiles were described using profile function #4 (Thompson *et al.*, 1987; Finger *et al.*, 1994), which includes the Stephens (1999) anisotropic strain broadening model. The background was modeled using a four-term shifted Chebyshev polynomial, with a four-term diffuse scattering function to model the Kapton capillary and any amorphous component. A second-order spherical harmonic model was included; the refined texture index was only 1.005, so preferred orientation was not significant. The final refinement of 122 variables using 27 059 observations (27 001 data points and 58 restraints) yielded the residuals $R_{wp} = 0.0608$, $R_p = 0.0484$, and $\chi^2 = 1.800$. The largest peak (0.07 Å from Ca20) and hole (2.19 Å from O35) in the difference Fourier map were 0.27 and $-0.24\ e$Å^{-3}, respectively. The Rietveld plot is included as Figure 2(c). The largest errors in the fit are in the shapes of some of the low-angle peaks.

DFT calculations

Density functional geometry optimizations (fixed experimental unit cells) were carried out using CRYSTAL14 (Dovesi *et al.*, 2014). The basis sets for the H, C, and O atoms were those of Gatti *et al.* (1994), and for Ca atoms was that of Catti *et al.* (1991). The calculations were run on eight 2.1 GHz Xeon cores (each with 6 Gb RAM) of a 304-core Dell Linux cluster at IIT, used eight k-points and the B3LYP functional, and took ∼1–15 days (22 h for the hexahydrate, 361 h for the new tetrahydrate, 145 h for ISEQIH, and 60 h for anhydrous).

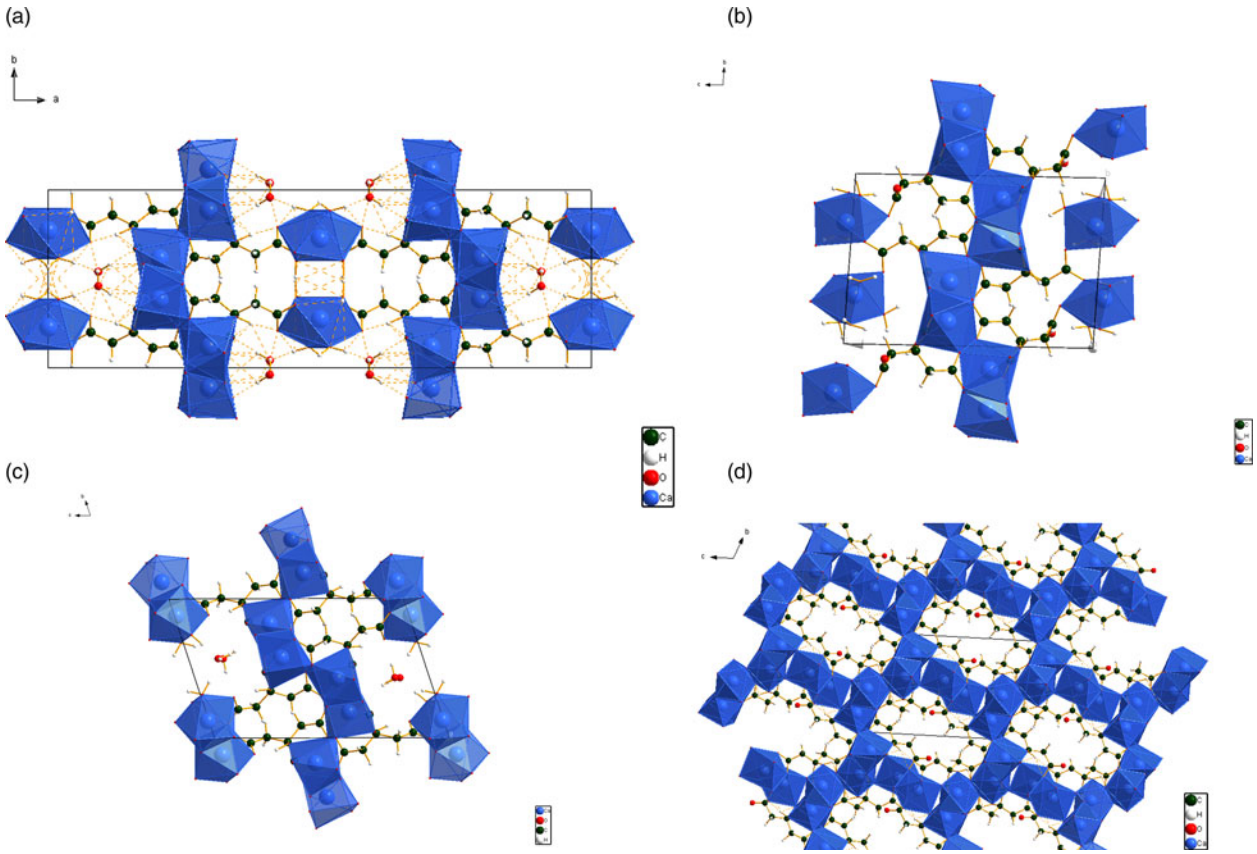


Figure 4. (Colour online) (a) The DFT-optimized crystal structure of calcium citrate hexahydrate, viewed down the c-axis. (b) The DFT-optimized crystal structure of the new polymorph of calcium citrate tetrahydrate, viewed down the a-axis. (c) The DFT-optimized crystal structure of the ISEQIH polymorph of calcium citrate tetrahydrate, viewed down the a-axis. (d) The DFT-optimized crystal structure of anhydrous calcium citrate, viewed down the a-axis.

https://doi.org/10.1017/S0885715618000283 Published online by Cambridge University Press

For $Ca_3(C_6H_5O_7)_2(H_2O)_4$, a density functional optimization (fixed experimental unit cell) was also carried out using VASP (Kresse and Furthmüller, 1996) through the MedeA graphical interface (Materials Design, 2016). The calculation was carried out on eight 2.4 GHz processors (each with 4 Gb RAM) of a 64-processor HP Proliant DL580 Generation 7 Linux cluster at North Central College. The calculation used the GGA–PBE functional, a planewave cut-off energy of 400 eV, and a *k*-point spacing of 0.5 $Å^{-1}$ (four *k*-points), and took 3.5 h.

III. RESULTS AND DISCUSSION

The refined atom coordinates of calcium citrate hexahydrate, calcium citrate tetrahydrate (both this form and ISEQIH), and anhydrous calcium citrate and the coordinates from the DFT optimizations are reported in the CIFs attached as Supplementary Material. The root-mean-square Cartesian displacement of the non-hydrogen atoms in the hexahydrate is only 0.086 Å [Figure 3(a)]. The excellent agreement between the refined and optimized structures is evidence that the experimental structure is correct (van de Streek and Neumann, 2014). The root-mean-square (RMS) displacement in the tetrahydrate is 0.652 Å, well outside the threshold for correct powder structures. The Ca positions are similar, as are the general positions of the citrate anions. The orientation of the O15–C6–O16 carboxyl group is unusual in the refined structure. The positions and orientations of the O13–C5–O14 and O33–C25–O34 carboxyl groups differ considerably between the refined and optimized structures. The RMS displacement in ISEQIH is only 0.059 Å, as expected for a correct single crystal structure. The RMS displacement in anhydrous calcium citrate is 0.364 Å, at the edge of correct powder structures. Although there are differences in the positions and orientations of carboxyl groups, the refined and optimized structures are quite similar. The following discussion uses the DFT-optimized structures, as I consider them to be more reliable.

Almost all of the bond distances, bond angles, and torsion angles in the citrate anions fall within the normal ranges indicated by a Mercury Mogul Geometry check (Macrae *et al.*, 2008). The C2–C3–C4 angle of 123° in the tetrahydrate, the C2–C3–C4–C5 torsion angle of 36° in the tetrahydrate, and the C2–C3–C4–C5 torsion angle of 131° in anhydrous calcium citrate are flagged as unusual. In the hexahydrate, the single citrate is in the *trans*/*trans* conformation, which is one of the two low-energy conformations of a citrate anion (Rammohan and Kaduk, 2018). In the tetrahydrate and anhydrous compounds, one of the two citrate anions is in the *trans*/*trans* conformation, but the other (as noted above) lies outside the usual distribution of *trans*/*trans* and *trans*/*gauche* conformations. In ISEQIH, some of the C-C-C-C torsional angles are also slightly unusual. Presumably, the coordination to Ca and hydrogen bonding has caused the citrate anions to distort slightly.

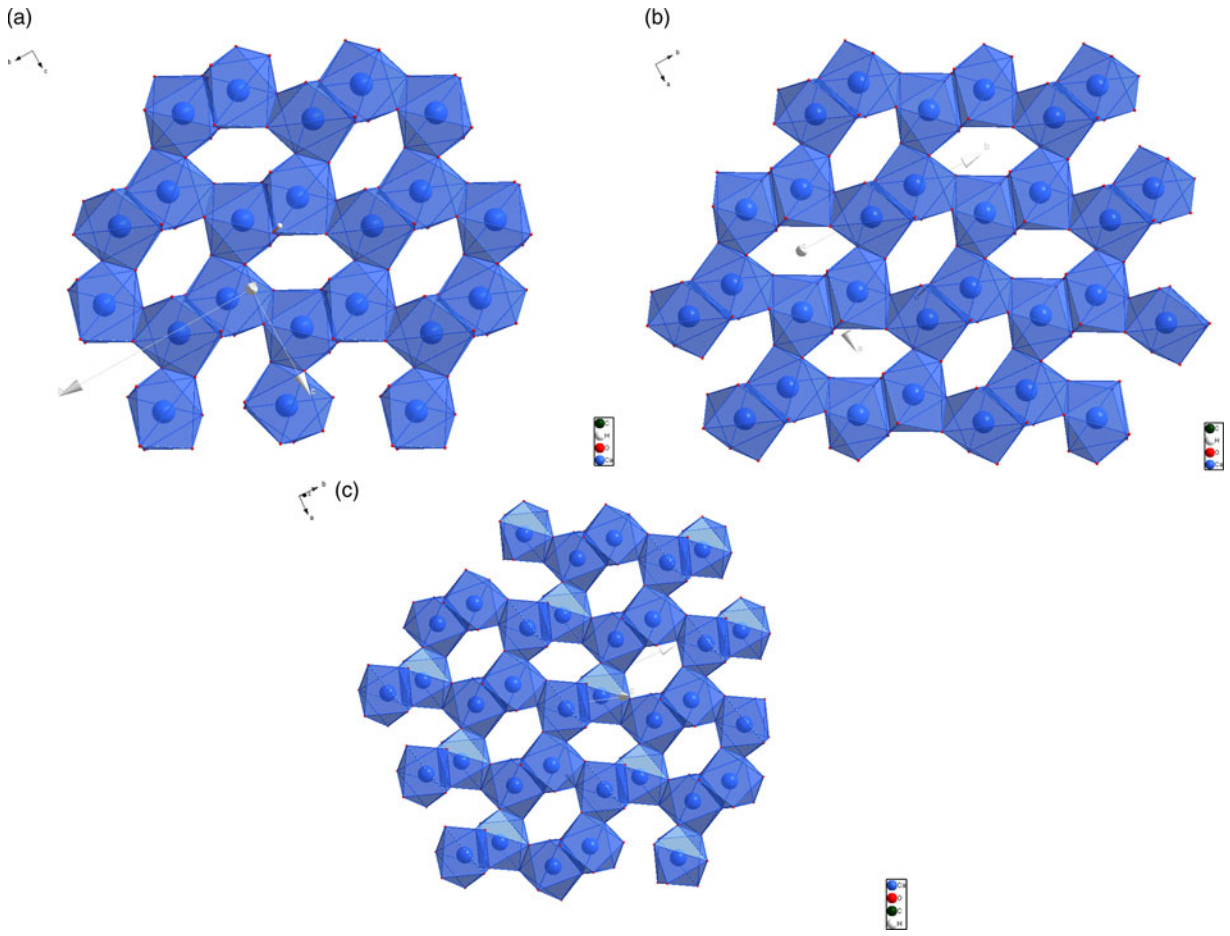


Figure 5. (Colour online) (a) The edge-sharing layer in calcium citrate hexahydrate. (b) The edge-sharing layer in the new polymorph of calcium citrate tetrahydrate. (c) The edge-sharing layer in the ISEQIH polymorph of calcium citrate tetrahydrate.

https://doi.org/10.1017/S0885715618000283 Published online by Cambridge University Press

TABLE II. Hydrogen bonds (CRYSTAL14) in the crystal structure of $Ca_3(C_6H_5O_7)_2(H_2O)_6$.

H-bond	D–H (Å)	H···A (Å)	D···A (Å)	D–H···A (°)	Overlap (*e*)	*E* (k m^{-1})
O23–H29···O16	0.975	1.867	2.822	165.6	0.044	11.5
O23–H28···O14	0.975	1.844	2.777	159.2	0.039	10.8
O22–H27···O22	0.964	2.171	2.796	121.4	0.032	9.8
O22–H26···O23	1.006	1.588	2.588	171.6	0.082	15.7
O21–H25···O13	0.978	1.884	2.856	172.2	0.051	12.3
O21–H24···O13	0.983	1.724	2.707	179.0	0.063	13.7
C4–H9···O16*	1.094	2.417	2.811	99.4	0.014	
C2–H7···O11	1.094	2.570	3.241	118.7	0.010	

*Intramolecular.

TABLE III. Hydrogen bonds (CRYSTAL14) in the crystal structure of the new polymorph of $Ca_3(C_6H_5O_7)_2(H_2O)_4$.

H-bond	D–H (Å)	H···A (Å)	D···A (Å)	D–H···A ()	Overlap (*e*)	*E* (k m^{-1})
O43–H51···O42	0.982	1.918	2.854	158.3	0.029	9.3
O42–H49···O13	0.998	1.673	2.654	166.8	0.056	12.9
O42–H48···O43	0.972	2.081	2.885	138.9	0.022	8.1
O41–H47···O17	0.976	1.801	2.775	175.4	0.039	10.8
O41–H46···O34	0.974	2.072	2.599	112.0	0.010	5.5
O41–H46···O35	0.974	2.189	2.707	150.0	0.009	5.2
O40–H45···O34	0.966	2.566	3.224	125.4	0.010	5.5
O40–H44···O33	0.985	1.738	2.715	170.5	0.038	10.6
O37–H38···O14	0.973	2.020	2.969	164.7	0.035	10.2
O17–H18···O13	0.983	1.801	2.721	154.6	0.045	11.6

TABLE IV. Hydrogen bonds (CRYSTAL09) in the crystal structure of the ISEQIH polymorph of $Ca_3(C_6H_5O_7)_2(H_2O)_4$.

H-bond	D–H (Å)	H···A (Å)	D···A (Å)	D–H···A (°)	Overlap (*e*)	*E* (k m^{-1})
O33–H51···O17	0.971	2.265	3.188	158.2	0.025	8.6
O33–H50···O32	0.989	1.739	2.727	176.7	0.069	14.4
O32–H49···O18	0.978	2.169	3.022	144.9	0.027	9.0
O32–H48···O4	0.979	1.917	2.888	171.1	0.047	11.8
O19–H39···O16*	0.999	1.599	2.523	151.5	0.068	14.3
O12–H38···O4*	0.990	1.715	2.617	149.5	0.063	13.7
O7–H37···O32	0.978	1.832	2.803	171.4	0.052	12.5
O7–H36···O5	0.977	1.930	2.875	162.1	0.055	12.8
O5–H35···O33	0.988	1.773	2.725	160.6	0.065	13.9
O5–H34···O33	0.985	1.850	2.810	163.7	0.056	12.0

*Intramolecular.

TABLE V. Hydrogen bonds (CRYSTAL14) in the crystal structure of $Ca_3(C_6H_5O_7)_2$.

H-bond	D–H (Å)	H···A (Å)	D···A (Å)	D–H···A (°)	Overlap (*e*)	*E* (k m^{-1})
O37–H38···O14	0.980	1.899	2.860	166.2	0.046	11.7
O17–H18···O31	0.981	1.938	2.883	160.8	0.053	12.6
C22–H27···O11	1.094	2.447	3.223	126.8	0.014	
C4–H10···O33	1.095	2.308	3.264	144.8	0.023	
C2–H8···O33	1.095	2.378	3.336	145.3	0.017	

TABLE VI. Quantitative analysis of commercial calcium citrate supplements. The concentrations are relative concentrations of the crystalline components, determined by Rietveld refinements.

Supplement	Citracal + D3	Walgreen's	21st Century
$Ca_3(cit)_2(H_2O)_4$	94.2(1)	95.8(1)	87.4(2)
new ISEQIH	–	3.0(2)	12.6(3)
Sum	94.2	98.8	100.0
Package info.	82.56	79.85	83.66
Poly(ethylene glycol)	5.5(3)	0.8(1)	–
Calcite	0.3(1)	0.3(1)	–

In the hexahydrate, Ca19 is 8-coordinate (bond valence sum = 2.13), and is bonded to only citrate oxygens. Ca20 is also 8-coordinate (bond valence sum = 2.19) and is bonded to four water molecules and four carboxylate oxygens. The water molecule O23 is not coordinated to Ca. In the new tetrahydrate, Ca19 and Ca20 (bond valence sums 2.14 and 2.24) are 8-coordinate, and bonded only to citrate oxygens. The third Ca39 is 7-coordinate (bond valence sum 1.92), and coordinated to three citrate oxygens and four water molecules. The carboxylate oxygen O13 is not coordinated to Ca. In ISEQIH, all three Ca are 8-coordinate. Ca2 and Ca3 (bond valence

https://doi.org/10.1017/S0885715618000283 Published online by Cambridge University Press

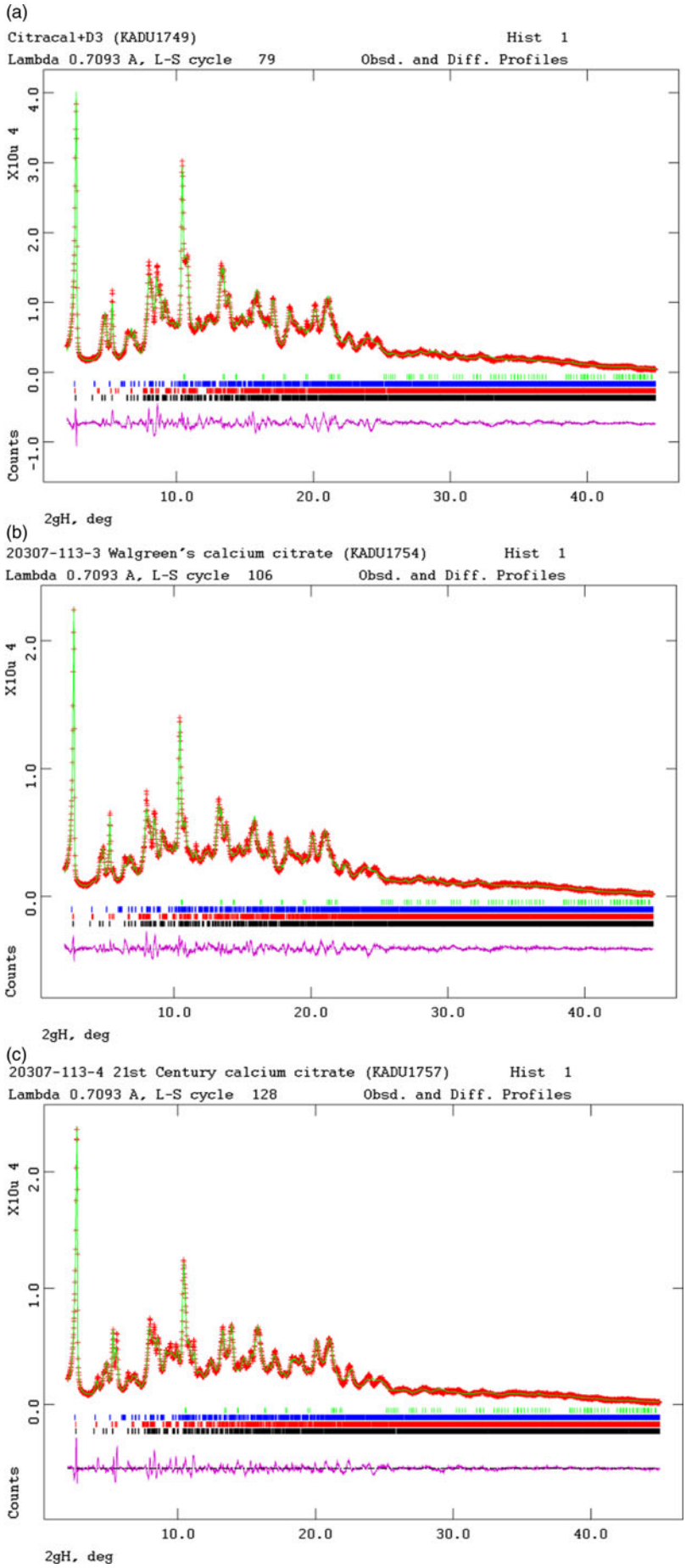


Figure 6. (Colour online) Rietveld plots for the refinement of three commercial calcium citrate supplements. The red crosses represent the observed data points, and the green line is the calculated pattern. The magenta curve is the difference pattern, plotted at the same vertical scale as the other patterns. The row of black tick marks indicates the calculated reflection positions for the new form, the red tick marks indicate peaks for the known ISEQIH structure, the blue tick marks indicate positions for poly(ethylene glycol) (CSD Refcode LILYOU01, and the green tick marks indicate the peaks for calcite. (A) Citracal + D3. (B) Walgreen's calcium citrate. (C) 21st Century calcium citrate.

https://doi.org/10.1017/S0885715618000283 Published online by Cambridge University Press

sums 2.22 and 2.20) are bonded only to carboxylate oxygens. Ca1 (bond valence sum 2.19) is bonded to six citrate oxygens and two water molecules. The water molecules O32 and O33 are not coordinated to Ca. The differences in coordination result in small differences in lattice parameters (Table I). In anhydrous calcium citrate, Ca19 and Ca20 are 8-coordinate (bond valence sums 2.09 and 2.16), while Ca39 is only 7-coordinate (bond valence sum 1.96). In three of the compounds, the Mulliken overlap populations in the Ca–O bonds range from 0.01 to 0.03 electrons, indicating a small degree of covalent character. In the new tetrahydrate, the overlap populations are slightly negative, indicating that the bonding is ionic.

A citrate anion is normally considered to be a good chelating agent, and several sorts of chelation are observed in these compounds. A carboxylate group acts as a bidentate ligand to a single Ca. Often, this chelation is accompanied by additional coordination to Ca on one or both of the carboxylate oxygens. All of these compounds contain at least one instance of triple chelation from a terminal carboxylate, the central carboxylate, and the hydroxyl group of a citrate.

The four crystal structures are illustrated in Figures 4(a)–4(d). A prominent feature of the hexahydrate and tetrahydrate structures is a layer of edge-sharing Ca coordination polyhedra [Figures 5(a)—5(c)]. Superposition of these layers shows that they are very similar, if not identical. The Ca which is coordinated by the water molecules is isolated from these layers. The persistence of the layers suggests that the mechanisms of dehydration and polymorph conversion involve the non-layer Ca and the water molecules. The same layer is present in the ISEQIH structure. The structure of anhydrous calcium citrate is a three-dimensional network of edge-sharing Ca coordination polyhedra [Figure 4(d)]; apparently, the layers have condensed, also involving the isolated Ca in the framework.

Analysis of the contributions to the total crystal energy using the Forcite module of Materials Studio (Dassault, 2014) suggests that bond distance, angle, and torsion distortion terms are small contributions to the intramolecular deformation energy. The intermolecular energy is dominated by electrostatic attractions, which in this force-field-based analysis include hydrogen bonds. The hydrogen bonds are better analyzed using the results of the DFT calculations.

As expected, hydrogen bonds are important in the structures of the hydrated compounds (Tables II, III, and IV). Almost all of the water molecules act as hydrogen bond donors. Only the H51 hydrogen atom in the current tetrahydrate does not participate in an O–H···O hydrogen bond. It does, however, seem to participate in two bonding interactions to H10 and C4 (Mulliken overlap populations 0.021 and 0.013 electrons, respectively). Hydrogen bonding is naturally less important in anhydrous calcium citrate (Table V), in which the hydroxyl groups form intermolecular hydrogen bonds and some weak C–H···O hydrogen bonds contribute to the crystal energy.

The Bravais–Friedel–Donnay–Harker (Bravais, 1866; Friedel, 1907; Donnay and Harker, 1937; calculated in *Mercury*) morphology suggests that we might expect platy morphology for all of these compounds, as expected from the layered nature of the structures. The principal faces are expected to be {200}, {001}, {001}, and {001} for the hexahydrate, the two polymorphs of tetrahydrate, and anhydrous calcium citrate respectively. Packing the capillary with the new tetrahydrate required much more tamping than for the hexahydrate and anhydrous material, so the observed larger degree of texture in the new pattern is reasonable.

Knowledge of the crystal structure of the major polymorph of calcium citrate tetrahydrate permits determination of the relative concentrations of the crystalline components of the commercial supplements by the Rietveld method (Table VI and Figure 6). Two of the three supplements contain both polymorphs, with ISEQIH as a minor component. The Citracal + D_3 also contains small concentrations of poly(ethylene glycol) (PEG) and calcite. It is worth noting that the PEG pattern is included only in the most-recent release of the Powder Diffraction File, providing a strong reason to update the database annually. The information on the packages (combined with the weights of the tablets) suggests that the calcium citrate tetrahydrate concentration in the tablets is ∼80 wt%. The labels indicate that the tablets contain additional compounds, most of which are expected to be amorphous: microcrystalline cellulose, cholecalciferol, croscarmellose sodium, *dl*-α-tocopherol, gum arabic, hydroxypropylmethylcellulose, magnesium silicate, stearic acid, magnesium stearate, maltodextrin, medium chain triglycerides, polydextrose, poly (vinyl alcohol), oligofructose-enriched inulin, polyvinylpyrrolidone, propylene glycol dicaprylate/dicaprate, silicon dioxide, titanium dioxide, talc, sodium ascorbate, starch, sucrose, sunflower oil, tricalcium phosphate, polysorbate, and vitamin D_3. Using the gravimetric concentrations of calcium citrate tetrahydrate, we can re-scale the apparent concentrations of the crystalline components, and determine the total concentration of amorphous species in these tablets.

SUPPLEMENTARY MATERIAL

The supplementary material for this article can be found at https://doi.org/10.1017/S0885715618000283

ACKNOWLEDGEMENTS

Use of the Advanced Photon Source at Argonne National Laboratory was supported by the U. S. Department of Energy, Office of Science, Office of Basic Energy Sciences, under Contract No. DE-AC02-06CH11357. I thank Lynn Ribaud and Saul Lapidus for their assistance in data collection, Andrey Rogachev for the use of computing resources at IIT, and Jose Orozco at IIT for TGA.

Altomare, A., Cuocci, C., Giacovazzo, C., Moliterni, A., Rizzi, R., Corriero, N., and Falcicchio, A. (**2013**). "EXPO2013: a kit of tools for phasing crystal structures from powder data," J. Appl. Crystallogr. **46**, 1231–1235.

Bannister, F. A. (**1936**). "Report on some crystalline components of the Weddell Sea deposits," Discov. Rep. **13**, 60–69.

Bravais, A. (**1866**). *Etudes Cristallographiques* (Gauthier Villars, Paris).

Catti, M., Dovesi, R., Pavese, A., and Saunders, V. R. (**1991**). "Elastic constants and electronic structure of fluorite (CaF_2): an ab initio Hartree-Fock study," J. Phys. Condens. Matter **3**, 4151–4164.

Dassault Systèmes (**2014**). *Materials Studio* 8.0 (BIOVIA, San Diego, CA).

Donnay, J. D. H., and Harker, D. (**1937**). "A new law of crystal morphology extending the law of Bravais," Amer. Mineral. **22**, 446–467.

Dovesi, R., Orlando, R., Erba, A., Zicovich-Wilson, C. M., Civalleri, B., Casassa, S., Maschio, L., Ferrabone, M., De La Pierre, M., D-Arco, P., Noël, Y., Causà, M., and Kirtman, B. (**2014**). "CRYSTAL14: a program for the ab initio investigation of crystalline solids," Int. J. Quantum Chem. **114**, 1287–1317.

https://doi.org/10.1017/S0885715618000283 Published online by Cambridge University Press

Favre-Nicolin, V., and Černý, R. (**2002**). "FOX, free objects for crystallography: a modular approach to ab initio structure determination from powder diffraction," J. Appl. Crystallogr. **35**, 734–743.

Fawcett, T. G., Kabekkodu, S. N., Blanton, J. R., and Blanton, T. N. (**2017**). "Chemical analysis by diffraction: the Powder Diffraction File™," Powder Diffr. **32**, 63–71.

Finger, L. W., Cox, D. E., and Jephcoat, A. P. (**1994**). "A correction for powder diffraction peak asymmetry due to axial divergence," J. Appl. Crystallogr. **27**(6), 892–900.

Friedel, G. (**1907**). "Etudes sur la loi de Bravais," Bull. Soc. Fr. Mineral. **30**, 326–455.

Gatti, C., Saunders, V. R., and Roetti, C. (**1994**). "Crystal-field effects on the topological properties of the electron-density in molecular crystals - the case of urea," J. Chem. Phys. **101**, 10686–10696.

Groom, C. R., Bruno, I. J., Lightfoot, M. P., and Ward, S. C. (**2016**). "The Cambridge structural database," Acta Crystallogr. Sect. B: Struct. Sci., Cryst. Eng. Mater. **72**, 171–179.

Herdtweck, E., Kornprobst, T., Sieber, R., Straver, L., and Plank, J. (**2011**). "Crystal structure, synthesis, and properties of *tri*-calcium *di*-citrate *tetra*-hydrate $[Ca_3(C_6H_5O_7)_2(H_2O)_2]\cdot 2H_2O$," Z. Anorg. Allg. Chem. **637**, 655–659.

Kresse, G., and and Furthmüller, J. (**1996**). "Efficiency of ab-initio total energy calculations for metals and semiconductors using a plane-wave basis set," Comput. Mater. Sci. **6**, 15–50.

Larson, A. C., and Von Dreele, R. B. (**2004**). *General Structure Analysis System,* (*GSAS*) (Los Alamos National Laboratory Report LAUR 86-784), Los Alamos, New Mexico.

Lee, P. L., Shu, D., Ramanathan, M., Preissner, C., Wang, J., Beno, M. A., Von Dreele, R. B., Ribaud, L., Kurtz, C., Antao, S. M., Jiao, X., and Toby, B. H. (**2008**). "A twelve-analyzer detector system for high-resolution powder diffraction," J. Synch. Rad. **15**(5), 427–432.

Macrae, C. F., Bruno, I. J., Chisholm, J. A., Edington, P. R., McCabe, P., Pidcock, E., Rodriguez-Monge, L., Taylor, R., van de Streek, J., and Wood, P. A. (**2008**). "Mercury CSD 2.0 – new features for the visualization and investigation of crystal structures," J. Appl. Crystallogr. **41**, 466–470.

Materials Design (**2016**). *MedeA 2.2.0* (Materials Design Inc., Angel Fire NM).

Mazaj, M., Kaucic, V., Golobic, A., and Zabukovec Logar, N. (**2012**). "A new layered Ca-succinate coordination polymer," Acta Crystallogr. **C68**, m4–m6.

MDI (**2016**). *Jade 9.7* (Materials Data. Inc., Livermore, CA).

Poganis, E. M., and Shaw, E. H. (**1957**). "The unit cell dimensions of tricalcium citrate tetrahydrate," Proc. South Dakota Acad. Sci. **36**, 56–59.

Rammohan, A., and Kaduk, J. A. (**2018**). "Crystal structures of alkali metal (Group 1) citrate salts", Acta Crystallogr. Sect. B: Cryst. Eng. Mater./ Acta Crystallogr. Sect. C: Struct. Chem. https://doi.org/10.1107/S2052520618002330.

Stephens, P. W. (**1999**). "Phenomenological model of anisotropic peak broadening in powder diffraction," J. Appl. Crystallogr. **32**, 281–289.

Thompson, P., Cox, D. E., and Hastings, J. B. (**1987**). "Rietveld refinement of Debye-Scherrer synchrotron X-ray data from Al_2O_3," J. Appl. Crystallogr. **20**(2), 79–83.

Toby, B. H. (**2001**). "EXPGUI, a graphical user interface for GSAS," J. Appl. Crystallogr. **34**, 210–213.

Tondapu, P., Provost, D., Adams-Huet, B., Sims, T., Chang, C., and Sakhaee, K. (**2009**). "Comparison of the absorption of calcium carbonate and calcium citrate after roux-en-Y gastric bypass," Obes. Surg. **19**, 1256–1261.

van de Streek, J., and Neumann, M. A. (**2014**). "Validation of molecular crystal structures from powder diffraction data with dispersion-corrected density functional theory (DFT-D)," Acta Cryst. Sect. B: Struct. Sci., Cryst. Eng. Mater. **70**(6), 1020–1032.

Wang, J., Toby, B. H., Lee, P. L., Ribaud, L., Antao, S. M., Kurtz, C., Ramanathan, M., Von Dreele, R. B., and Beno, M. A. (**2008**). "A dedicated powder diffraction beamline at the advanced photon source: commissioning and early operational results," Rev. Sci. Inst. **79**, 085105.

https://doi.org/10.1017/S0885715618000283 Published online by Cambridge University Press